

# Cuprate Fermi orbits and Fermi arcs: the effect of short-range antiferromagnetic order

N. Harrison, R.D. McDonald, and J. Singleton

National High Magnetic Field Laboratory, Los Alamos National Laboratory, MS E536, Los Alamos, New Mexico 87545

(Dated: October 26, 2018)

We consider the effect of a short antiferromagnetic correlation length  $\xi$  on the electronic band-structure of the underdoped cuprates. Starting with a Fermi-surface topology consistent with that detected in magnetic-quantum-oscillation experiments, we show that a reduced  $\xi$  gives an asymmetric broadening of the quasiparticle dispersion, resulting in simulated ARPES data very similar to those observed in experiment. Predicted features include the presence of ‘Fermi arcs’ close to  $a\mathbf{k} = (\pi/2, \pi/2)$ , where  $a$  is the in-plane lattice parameter, without the need to invoke a  $d$ -wave pseudogap order parameter. The statistical variation in the  $k$ -space areas of the reconstructed Fermi-surface pockets causes the quantum oscillations to be strongly damped, even in very strong magnetic fields, in agreement with experiment.

Magnetic quantum oscillations such as the de Haas-van Alphen and Shubnikov-de Haas effects are acknowledged to be the most reliable method to determine the detailed low-temperature Fermi-surface topologies of metals [1, 2]. Recently, Shubnikov-de Haas oscillations have been observed in the underdoped cuprate superconductors  $\text{YBa}_2\text{Cu}_3\text{O}_{6.5}$  [3] and  $\text{YBa}_2\text{Cu}_4\text{O}_8$  [4, 5]; the data reveal quasi-two-dimensional Fermi-surface sections with cross-sections that are  $\sim 2 - 2.4\%$  of the area of the Brillouin zone. This result is consistent with a picture [3] in which antiferromagnetic order breaks translational symmetry, reconstructing the large Fermi surface seen in overdoped cuprates [6] into four small, symmetry-related pockets. At first sight, this conclusion is at variance with angle-resolved photo-emission (ARPES) experiments [7, 8], which find only so-called ‘Fermi arcs’. However, we show here that the quantum-oscillation and ARPES results are compatible. Starting with a Fermi surface consistent with the quantum-oscillation experiments, we show that a reduced antiferromagnetic correlation length  $\xi$  gives an asymmetric broadening of the quasiparticle dispersion, resulting in predicted ARPES spectral weights similar to those observed in experiment.

The breaking of translational symmetry due to antiferromagnetism can be described by a modulation vector  $\mathbf{Q}$  that is sharply defined in an ideal antiferromagnet [9]; this is the case in the parent Mott-insulating phase of the cuprates [10], realized for hole dopings  $p \lesssim 0.05$ . However, in the underdoped regime ( $0.05 \lesssim p \lesssim 0.2$ ), slow antiferromagnetic fluctuations, detected in neutron-scattering experiments, cause  $\mathbf{Q}$  to become subject to statistical variations over a wide range of conditions [10, 11]. At temperatures  $T \lesssim 10$  K, the fluctuations become sufficiently slow for the system to resemble a glassy state comprising antiferromagnetic microdomains with lifetimes  $\tau_f \approx 10^{-9}$  s [12]. This lifetime exceeds by several orders of magnitude both that for the re-equilibration of the Fermi sea occurring in ARPES experiments ( $\tau_r \sim 10^{-15}$  s) [7, 8] and the period of quasiparticle Fermi-surface orbits in strong magnetic fields ( $2\pi\omega_c^{-1} \sim 10^{-12}$  s, where  $\omega_c$  is the cyclotron

frequency [3, 4]). Therefore, from the perspective of both experimental techniques, quasiparticles can be considered to propagate through a glassy antiferromagnetic medium in which the staggered magnetization is quasi-static and periodic over distances of order  $\xi$ .

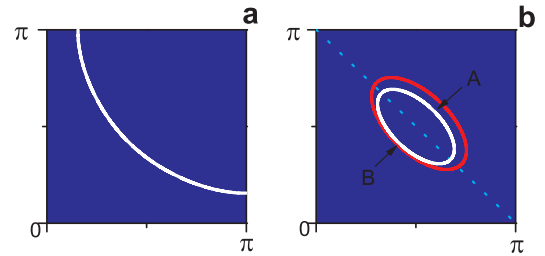


FIG. 1: Quadrant of a notional cuprate Fermi surface for  $p = 0.095$  doped holes per planar Cu atom. **a.** The Fermi surface given by Eq. 1 in the absence of ordering. **b.** The Fermi surface (white line) after reconstruction (*i.e.* folding about the dotted line) with respect to  $a\mathbf{Q} = a\mathbf{Q}_0 = (\pi, \pi)$  with  $\Delta = t_{10}$  in Eq. 2. The red line shows the corresponding Fermi surface for a slightly different  $\mathbf{Q}$ , shifted relative to  $\mathbf{Q}_0$ .

To see how ARPES and quantum oscillation experiments are affected by the short antiferromagnetic correlation lengths  $\xi$ , we consider a simplified, two-dimensional quasiparticle dispersion of the form

$$\varepsilon_{\mathbf{k}} = 2t_{10}(\cos ak_x + \cos ak_y) + 2t_{11}(\cos a(k_x + k_y) + \cos a(k_x - k_y)). \quad (1)$$

Eq. 1 gives rise to a large hole Fermi surface sheet centered on  $a\mathbf{k} = (\pi, \pi)$  for  $t_{10} < 0$ ,  $t_{11} \approx -0.34 \times t_{10}$  and  $p > 0$ ; this is approximately representative of cuprate Fermi surfaces in the absence of ordering [6]. Figure 1a shows a quadrant of such a Fermi surface for  $p = 0.095$  holes per Cu atom within the Cu-O planes. The entire Fermi surface accommodates  $1 + p$  holes per unit cell (in the absence of ordering), having a  $k$ -space cross-sectional area  $A_{\mathbf{k}} = 2\pi^2(1 + p)/a^2$ , where  $a$  is the in-plane lattice constant. The Fermi energy  $\varepsilon_F$  is obtained self-consistently from  $A_{\mathbf{k}} = \int \int f(\varepsilon_F - \varepsilon_{\mathbf{k}}) dk_x dk_y$ , where  $f(x)$  is the Fermi-Dirac distribution function with the double integration being performed within the first Brillouin zone.

The reconstruction of such a Fermi surface caused by long-range antiferromagnetic order is well understood [9]. The staggered magnetization  $\mathbf{m} = \mathbf{m}_0 \cos(\mathbf{r} \cdot \mathbf{Q})$  represents a new periodicity of the system that introduces a new, smaller Brillouin zone and causes the quasiparticle dispersion relationship (Eq. 1) to become gapped close to the zone boundaries by an energy  $2\Delta$ . In the weak-coupling limit,  $\Delta \ll 4t_{10}$ , the modified dispersion can be written

$$\varepsilon_{\mathbf{k}, \mathbf{Q}} \approx \frac{\varepsilon_{\mathbf{k}} + \varepsilon_{\mathbf{k}+\mathbf{Q}}}{2} \pm \sqrt{\left(\frac{\varepsilon_{\mathbf{k}} - \varepsilon_{\mathbf{k}+\mathbf{Q}}}{2}\right)^2 + \Delta^2}, \quad (2)$$

in the absence of an applied magnetic field [9, 13]. The white line in Fig. 1b shows one of the four equivalent Fermi-surface pockets that result for  $\Delta = t_{10}$  and  $a|\mathbf{Q}| = a|\mathbf{Q}_0| = |(\pi, \pi)|$  [14]. To accommodate  $p$  holes within the reduced Brillouin zone (bounded by the dotted line), each pocket has an area  $A_{\mathbf{k}, \mathbf{Q}_0} = \pi^2 p/a^2$  [15]. To conserve charge neutrality, the introduction of antiferromagnetic order is accompanied by a shift in Fermi energy from  $\varepsilon_F$  to  $\varepsilon_{F, \mathbf{Q}_0}$ ; hence  $A_{\mathbf{k}, \mathbf{Q}_0} = \frac{1}{4} \int \int f(\varepsilon_{F, \mathbf{Q}_0} - \varepsilon_{\mathbf{k}, \mathbf{Q}_0}) dk_x dk_y$ .

The parameters  $p = 0.095$  and  $\Delta = t_{10}$  used in Fig. 1b are chosen to mimic the experimental Fermi surfaces of  $\text{Ca}_{1.9}\text{Na}_{0.1}\text{CuO}_2\text{Cl}_2$  [7] and  $\text{YBa}_2\text{Cu}_4\text{O}_8$  [4] for which the corresponding quantum-oscillation frequency is  $F = hp/4ea^2 \approx 650$  T. Whereas the Mott insulating parent phase ( $p \lesssim 0.05$ ) may be understood within a strong-coupling description of antiferromagnetism [10, 17], the appropriate regime for  $p \approx 0.1$  remains a matter of conjecture [11]. In the strong coupling limit ( $\Delta \gg t_{10}$ ), the hole pockets at  $(\pi/2, \pi/2)$  would depart only marginally from the form depicted in Fig. 1b, the primary effect being to renormalize the widths of the upper and lower bands defined by Eq. 2. In the very weak coupling limit ( $\Delta/t_{10} \rightarrow 0$ ), however, in addition to the hole pockets at  $(\pi/2, \pi/2)$ , small electron pockets would appear at  $(\pi, 0)$ ; there is as yet no evidence for the latter pockets in quantum-oscillation data [4].

We model the effect of short correlation lengths using a probability distribution for  $\mathbf{Q}$  [18], as determined by neutron-scattering experiments [10]. As stated above, in ARPES and quantum-oscillation experiments we are in the limit  $\tau_f \gg \omega_c^{-1} \gg \tau_r$ , so that the distribution can be considered static:

$$p_{\mathbf{Q}} = \frac{K}{\xi^{-2} + (\mathbf{Q}_0 - \mathbf{Q})^2}, \quad (3)$$

with  $\int \int p_{\mathbf{Q}} dQ_x dQ_y = 1$  [19]. To help understand how the Fermi surface is modified by variations in  $\mathbf{Q}$ , the red curve in Fig. 1b shows how the pocket is deformed by a small shift of  $\mathbf{Q}$  relative to  $\mathbf{Q}_0$ . Whereas the ‘A’ branch of the Fermi-surface orbit (required by the translational symmetry of the new Brillouin zones) is strongly modified by this shift, the ‘B’ branch that corresponds more closely to the original Fermi surface is less altered. This is

true irrespective of the direction of the shift in  $\mathbf{Q}$ . Thus, the ‘B’ branch is more resilient against statistical variations in  $\mathbf{Q}$  than is ‘A’. On considering all possible values of  $\mathbf{Q}$  within this distribution, the resulting dispersion and Fermi surface become broadened; observables such as the photoemission spectral weight and Landau-level broadening can then be estimated by analogy with other types of “phase smearing” [1, 20].

ARPES provides information on  $\varepsilon_{\mathbf{k}}$  and the extent to which it is broadened by correlations or other factors, giving rise to a photoelectron intensity that is distributed in energy and  $k$ -space [7, 8, 21]. When the energy distribution curve is cut off by the Fermi-Dirac distribution, the rapidity with which the integrated intensity grows with  $\varepsilon_F - \varepsilon_{\mathbf{k}}$  close to the Fermi energy can be used to obtain a ‘Fermi surface intensity plot’ [7, 8, 21]. The discontinuous jump at  $\varepsilon_F$  encountered in conventional metals therefore gives rise to an associated spectral weight  $S_{\mathbf{k}} = \delta(\varepsilon_{\mathbf{k}} - \varepsilon_F)$  that is infinite at  $T = 0$  under ideal conditions. In actual experiments, however, with overpopped  $\text{Ti}_2\text{Ba}_2\text{CuO}_{6+\delta}$  providing a good example, the spectral weight at  $\varepsilon_F$  is broadened by finite temperature and self-energy effects and by instrumental energy resolution [21].

In the case of antiferromagnetism with a distribution of  $\mathbf{Q}$ , we determine the spectral weight from the convolution of  $\delta(\varepsilon_{\mathbf{k}, \mathbf{Q}} - \varepsilon_{F, \mathbf{Q}_0})$  with Eq. 3:

$$S_{\mathbf{k}, \mathbf{Q}_0} = \int \int \delta(\varepsilon_{\mathbf{k}, \mathbf{Q}} - \varepsilon_{F, \mathbf{Q}_0}) p_{\mathbf{Q}} dQ_x dQ_y. \quad (4)$$

The sensitivity of the reconstructed Fermi surface to statistical variations in  $\mathbf{Q}$  (i.e. Fig. 1b) introduces a strongly  $k$ -space dependent broadening of the spectral weight. Fig. 2 shows the spectral weight calculated using Eq. 4 for several different values of  $\xi$ . At large  $\xi$ , the spectral weight strongly resembles the outline of the Fermi surface depicted in white in Fig. 1b. As  $\xi$  becomes shorter, however, the spectral weight corresponding to the part of the Fermi surface produced by the  $k$ -space reconstruction (labeled ‘A’) fades to be replaced by a greater concentration along an arc of the original unreconstructed Fermi surface. At  $\xi = 10$  and  $20$  Å, the distribution of spectral weight closely resembles that observed in  $\text{Ca}_{1.9}\text{Na}_{0.1}\text{CuO}_2\text{Cl}_2$  (see Figs. 1b,c of Ref. [7]), for which  $p \approx 0.1$ . These values of  $\xi$  are in excellent agreement with neutron-scattering estimates made at the same nominal  $p$  in a variety of cuprates (at temperatures  $\sim$  tens of kelvin in zero applied magnetic field) [10].

The model reproduces the features seen in  $\text{Ca}_{1.9}\text{Na}_{0.1}\text{CuO}_2\text{Cl}_2$  and  $\text{Bi}_2\text{Sr}_2\text{CaCu}_2\text{O}_{8+\delta}$  ARPES data [7, 8]. Fig. 3a shows the angle ( $\theta$ ) dependence of the spectral weight from Fig. 2 ( $\xi = 10$  Å) tracing the  $\mathbf{k} = \mathbf{k}_F$  arc of the original unreconstructed Fermi surface in Fig. 1a. The sinusoidal variation of  $S_{\mathbf{k}_F, \mathbf{Q}_0}$  with  $\theta$  (Fig. 3a) and the strongly reduced gradient of the energy distribution intensity  $I$  with respect to  $\varepsilon$  at  $\mathbf{k}_{\pm 45^\circ}$  in Fig. 3b are very similar to ARPES data [7, 8].

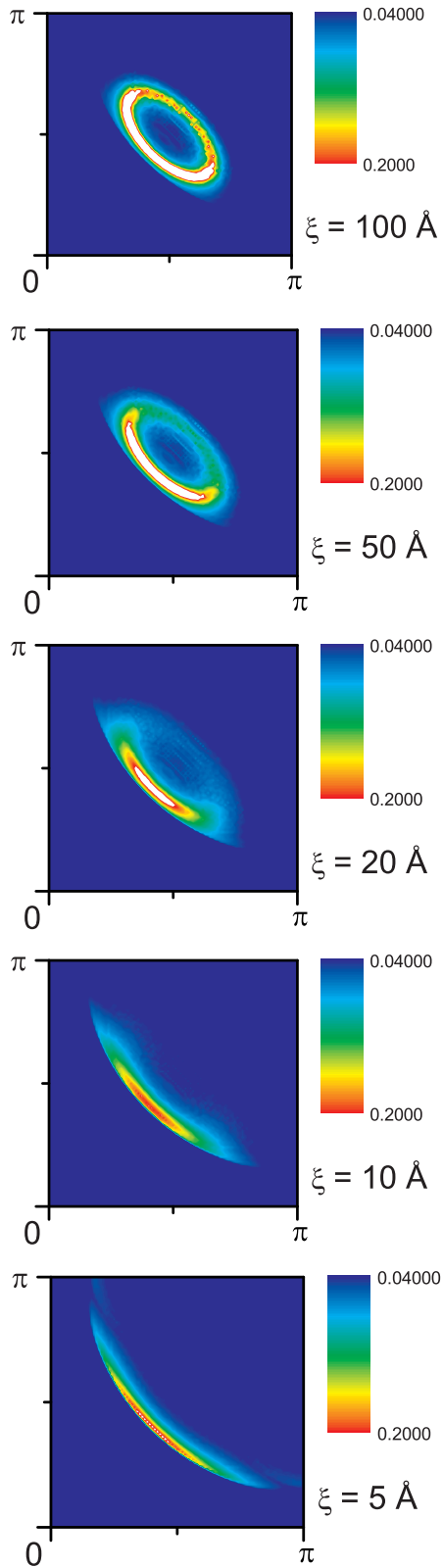


FIG. 2: Spectral weight calculated over a quadrant of the Fermi surface using Eq. 4 for different values of  $\xi$ . Since the continuous variables  $\mathbf{k}$  and  $\varepsilon$  are replaced by discrete quantities in the simulations, the delta function is replaced by a Kronecker delta.

Such features have been interpreted in terms of a ‘pseudogap’; note that our model shows that short-range antiferromagnetic order can also give the ‘illusion’ of a  $d$ -wave order parameter with a node at  $\theta = 0^\circ$  and antinodes at  $\theta = \pm 45^\circ$  (see inset) [7]. This is also shown in Fig. 3b that plots the energy distribution calculated using Eq. 4 at selected values  $\mathbf{k}_F$  along the arc of the unreconstructed Fermi surface. To simulate experimental curves, the spectral intensity is modulated by  $f(\varepsilon_{\mathbf{k}} - \varepsilon_F)$  at  $T = 0$  and broadened by an ‘instrumental resolution’ gaussian of width  $\approx \frac{1}{5}\Delta$ . When symmetrized [8], the energy distribution closely reproduces the apparent “pseudogap behavior” of  $\text{Bi}_2\text{Sr}_2\text{CaCu}_2\text{O}_{8+\delta}$  [8].

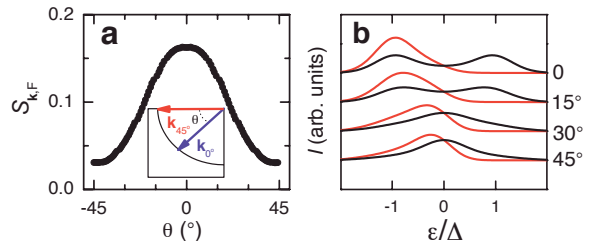


FIG. 3: **a** The approximately sinusoidal variation of the spectral weight in Fig. 2 ( $\xi = 10 \text{ \AA}$ ) with angle  $\theta$ , following the arc of the unreconstructed Fermi surface from Fig. 1a.  $\theta$  is the angle between the line linking  $(\pi, \pi)$  to  $(0, 0)$  and that linking  $(\pi, \pi)$  to the arc (inset). **b** Calculated energy distribution intensity at  $\mathbf{k}_F$  along the unreconstructed Fermi surface at different  $\theta$ . Red curves are calculations; black curves are “symmetrized” in the same manner as experimental data [8].

Quantum-oscillation experiments give a direct measure of  $A_{\mathbf{k}, \mathbf{Q}_0}$  (Fig. 1b) that is also subject to statistical variations. The probability distribution is given by

$$p_{A_{\mathbf{k}}} = \int \int \delta(A_{\mathbf{k}, \mathbf{Q}} - A_{\mathbf{k}}) p_{\mathbf{Q}} dQ_x dQ_y. \quad (5)$$

Fig. 4a shows Eq. 5 for several  $\xi$ ; the curves resemble the probability distributions caused by finite quasiparticle lifetime or other forms of disorder [1, 20], leading to a qualitatively similar Landau-level broadening and quantum-oscillation damping. Figure 4b shows predicted damping factors for the fundamental quantum-oscillation frequency  $F \approx 650 \text{ T}$  in  $\text{YBa}_2\text{Cu}_4\text{O}_8$  [4] and for the  $2F$  harmonic. The correlation lengths  $\xi \approx 10$  and  $20 \text{ \AA}$  that are best able to reproduce the  $\mathbf{k}$ -dependent spectral weight of  $\text{Ca}_{1.9}\text{Na}_{0.1}\text{CuO}_2\text{Cl}_2$  [7] in Fig. 2 cause too much damping to mimic the data of Ref. [4]; a damping factor  $\sim 10^{-3}$  is the typical cutoff for observable quantum oscillations, corresponding to  $\xi \approx 90 \text{ \AA}$ . An upper limit of  $\xi \lesssim 400 \text{ \AA}$  comes from the absence of harmonics in the data, normally abundant in quasi-two dimensional metals [22]; *i.e.*  $90 \lesssim \xi \lesssim 400 \text{ \AA}$ . The observation of quantum oscillations in  $\text{YBa}_2\text{Cu}_3\text{O}_{6.5}$  [3] and  $\text{YBa}_2\text{Cu}_4\text{O}_8$  [4] therefore suggests a correlation length several times longer than that in ARPES experiments.

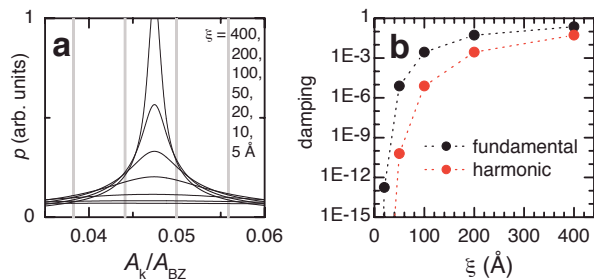


FIG. 4: **a** The  $A_{\mathbf{k},\mathbf{Q}_0}$  probability distribution for several values of  $\xi$ . Grey lines mark the positions of the ideal  $\delta$ -function Landau levels for a field of 80 T expected in this quasi-two dimensional metal were long-range antiferromagnetic order established. These would furnish quantum oscillations periodic in  $1/B$ , rich in harmonic content. **b** A plot of the corresponding damping factor versus  $\xi$  for the fundamental frequency (black) and harmonic (red) resulting from the convolution of the probability distribution with the  $\delta$ -function Landau levels.

The differences in  $\xi$  result from the contrasting conditions under which ARPES and quantum-oscillation experiments are performed. Whereas ARPES experiments are performed at tens of kelvins and zero magnetic field, quantum-oscillation experiments are made at liquid helium temperatures in the strongest fields available. Abundant neutron scattering data on Sr- and O-doped  $\text{La}_2\text{CuO}_4$  (as well as electron-doped cuprates) show an enhancement of antiferromagnetism and/or its associated correlation length at liquid  $^4\text{He}$  temperatures under magnetic fields [23], with values as large as  $\xi \approx 400$  Å reported [23]. While similar neutron-scattering data are unavailable for the two systems ( $\text{YBa}_2\text{Cu}_3\text{O}_{6.5}$  and  $\text{YBa}_2\text{Cu}_4\text{O}_8$ ) in which quantum oscillations are observed, alternative experimental techniques do provide evidence for field-induced antiferromagnetism [24]. These include nuclear magnetic resonance [25], muon spin rotation [26] and magnetic torque [27].

In conclusion, we show that the seemingly contradictory results of ARPES and quantum oscillation experiments on the underdoped cuprates can be brought into mutual agreement by considering the slow antiferromagnetic fluctuations with a short correlation length detected by neutron-scattering experiments. Whereas the correlation length is very short ( $10 \lesssim \xi \lesssim 20$  Å) in the normal state at zero magnetic field, it becomes enhanced ( $90 \lesssim \xi \lesssim 400$  Å) at liquid He temperatures in magnetic fields due to a field-induced stabilization of antiferromagnetism [16]. Short correlation lengths lead to a reduction in the spectral weight that is most pronounced close to  $(\pi, 0)$  on the unreconstructed Fermi surface, giving rise to the emergence of Fermi arcs near  $(\pi, \pi)$  in a qualitatively similar fashion to a  $d$ -wave order parameter. The effects described in this paper should also occur for other forms of ordering that lack long range periodicity, including stripes and/or charge order [7]. However, only antiferromagnetism is truly ubiquitous, giving rise to clear signatures in neutron-diffraction experiments in

all underdoped cuprates investigated.

We are very grateful to Ed Yelland, Chandra Varma and Louis Taillefer for stimulating discussions. This work is supported by the US Department of Energy (DoE) BES program ‘‘Science in 100 T’’. Work at NHMFL is carried out under the auspices of the National Science Foundation, DoE and the State of Florida.

- 
- [1] D. Shoenberg, *Magnetic Quantum Oscillations in Metals* (Cambridge University Press, 1984).
  - [2] A. Wasserman and M. Springford, *Adv. Phys.* **45**, 471 (1996); J. Singleton, *Rep. Prog. Phys.* **63**, 1111 (2000).
  - [3] N. Doiron-Leyraud *et al.*, *Nature* **447**, 565 (2007).
  - [4] E.A. Yelland *et al.*, preprint arXiv:0707.0057.
  - [5] A.F. Bangura *et al.*, preprint arXiv:0707.4461.
  - [6] N.E. Hussey *et al.*, *Nature* **425**, 814 (2003).
  - [7] K. M. Shen *et al.*, *Science* **307**, 901 (2005).
  - [8] A. Kanigel *et al.*, *Nature Phys.* **2**, 447 (2006).
  - [9] G. Grüner, *Rev. Mod. Phys.* **66**, 1 (1994); R.G. Goodrich *et al.*, *Phys. Rev. Lett.* **97**, 146404 (2006).
  - [10] A. P. Kampf, *Phys. Rep.* **249**, 219 (1994).
  - [11] R. J. Birgeneau *et al.*, *J. Phys. Soc. Japan* **75**, 111003 (2006).
  - [12] S. M. Hayden *et al.*, *Phys. Rev. Lett.* **66**, 821 (1991).
  - [13] The largest field applied (85 T [4]) is significantly lower than that required to polarize the Cu spins [10].
  - [14] For simplicity we assume  $a\mathbf{Q}_0 = (\pi, \pi)$  throughout. Whereas the actual  $\mathbf{Q}_0$  may become incommensurate for  $p \gtrsim 0.05$  [10], branch ‘B’ of the reconstructed Fermi surface is just as resilient to small changes in  $\mathbf{Q}_0$  as it is to small statistical variations in  $\mathbf{Q}$ . An incommensurate  $\mathbf{Q}_0$  leads to small differences (i.e. see Fig. 1b) in Fermi surface topology for large values of  $\xi$  that nevertheless become indiscernible for short values of  $\xi$ .
  - [15] The estimates of  $p$  from quantum-oscillation frequencies made in [3] and [4] are a factor 2 too large, through not allowing for the reduced Brillouin zone. See also [16].
  - [16] Wei-Qiang Chen *et al.*, preprint arXiv:0706.3556.
  - [17] S. A. Trugman, *Phys. Rev. Lett.* **65**, 500(1990).
  - [18] P.A. Lee *et al.*, *Phys. Rev. Lett.* **31**, 462 (1973).
  - [19] To avoid logarithmic divergences, the  $k$ -space integration of  $p\mathbf{Q}$  is cutoff at  $\pm\pi$ . This problem may also be avoided by adopting a Gaussian distribution [10].
  - [20] N. Harrison and J. Singleton, *J. Phys.: Cond. Matter* **13**, L463 (2001).
  - [21] M. Platié *et al.*, *Phys. Rev. Lett.* **95**, 077001 (2005).
  - [22] N. Harrison *et al.*, *Phys. Rev. B* **54** 9977 (1996)
  - [23] H. Kimura *et al.*, *Phys. Rev. B* **59**, 6517 (1999); B. Lake *et al.*, *Nature* **415**, 299 (2002); B. Lake *et al.*, *Phys. Stat. Sol. B* **241**, 1223 (2004); B. Khaykovich *et al.*, *Phys. Rev. B* **66**, 014528 (2002); M. Matsuura *et al.*, *Phys. Rev. B* **69**, 104510 (2004); J. E. Sonier *et al.*, *Physica C* **408-410**, 783 (2004); B. Khaykovich *et al.*, *Phys. Rev. B* **71**, 220508 (2005).
  - [24] Y. Zhang, E. Demler and S. Sachdev, *Phys. Rev. B* **66**, 094501 (2002).
  - [25] V.F. Mitrovic *et al.*, *Nature* **413**, 501 (2001).
  - [26] R.I. Miller *et al.*, *Phys. Rev. Lett.* **88**, 137002 (2002).
  - [27] T. Ishida *et al.*, *Physica C* **426-431**, 69 (2005).